

See discussions, stats, and author profiles for this publication at: <https://www.researchgate.net/publication/284701251>

Wavelet transform of acoustic emission signals

Article · January 1996

CITATIONS

119

READS

3,160

5 authors, including:



Kanji Ono

University of California, Los Angeles

156 PUBLICATIONS 4,365 CITATIONS

[SEE PROFILE](#)

Some of the authors of this publication are also working on these related projects:



Ancient metals [View project](#)

Wavelet Transform of Acoustic Emission Signals

Hiroaki Suzuki, Tetsuo Kinjo, Yasuhisa Hayashi, Mikio Takemoto and Kanji Ono with Appendix by Yasuhisa Hayashi

Abstract

Wavelet transform (WT) allows the determination of frequency spectrum as a function of time using short waveform segments or wavelets as the basis functions. Resultant mapping of wavelet coefficients in the frequency-time coordinate plane provides more informative characterization of acoustic emission (AE) signals than the power-density spectra from usual Fourier transform. A short tutorial on WT is included. A program for performing WT procedure has been developed and is given as Appendix. As an example, wavelet transform was performed on AE signals from a longitudinal glass-fiber reinforced composite sample under tensile loading. Obtained spectrograms were classified into four types and correlated to the fracture dynamics separately determined by radiation pattern and source simulation analyses. WT is demonstrated to be a powerful new analysis method in evaluating AE signals.

1. Introduction

In the analysis of acoustic emission (AE) signals, the Fourier transform (FT) or fast Fourier transform (which is an efficiently implemented algorithm for FT) is utilized often. Beside providing the frequency spectral information of a signal, FT is the key element of many pattern recognition analysis methods as well as source characterization algorithms. However, FT cannot generate time-dependence of the frequency spectrum because the exponential basis function, $\exp(-i\omega t)$, extends over the entire signal duration. Here, i is the imaginary sign and ω is the angular frequency, $2\pi f$.

The high frequency limit of the FT in the presently practiced digitized form (commonly known as discrete

Fourier transform) can be increased by increasing the rate of digitization according to the Nyquist theorem. In the FT, a signal of typically limited duration is extended in time to $\pm\infty$ by periodically repeating the signal. This periodicity defines the resolution of the FT. Thus, the frequency resolution can be improved by extending the duration of the signal analyzed. This, in turn, reduces the time resolution, because the obtained spectrum is for the entire duration. This is due to the Uncertainty Principle in time t and frequency f ; $\Delta t \Delta f \geq 1/4\pi$.

The short-time Fourier transform or windowed Fourier transform (WFT) overcomes the drawback of FT to some extent. It consists of multiplying a signal $s(t)$ with a short window function $w(t - \tau)$, centered at time, τ , and computing the Fourier transform of the product $s(t)w(t - \tau)$. The window, $w(t - \tau)$, is short relative to the signal duration. Gabor (1946) used the Gaussian function as the window function and this procedure is now known as Gabor transform. By the Gabor transform, one can estimate the frequency content of the signal $s(t)$ in the neighborhood of τ . The window width is constant in Gabor transform and is of the order of the period of the lowest frequency being analyzed, whether $s(t)$ around τ has a low or high frequency content. Thus, the uncertainty in time, Δt , is still substantial at higher frequencies. The application of WFT to AE signal analysis has been limited. Until recently, it was confined to only one oral presentation by Calros Salvado (of Rockwell International Science Center at the time) at one of the AEWG meetings. The voice-print or WFT's analog-equivalent was used by Green et al. (1962) in the analysis of AE signals from rocket motorcase testing.

The wavelet transform (WT) is a time-frequency transform of continuous (analog) or discrete (digitized) signals. It is described as a time-scale transform in the WT literature. The WT is a direct alternative to the windowed Fourier transform and has been applied to a number of areas, including data compression, image processing and time-frequency spectral estimation. Its theoretical foundation was developed by Morlet and Grossmann (1984). Daubechies (1988) and Mallat (1989) brought the concept of wavelets into digital signal processing. For recent monographs, see Chui (1992), Daubechies (1992) and Kaiser (1994). Within its short history, the WT has become an indispensable tool in various

Received May 12, 1996. Hiroaki Suzuki, Tetsuo Kinjo and Mikio Takemoto are affiliated with Faculty of Science and Engineering, Aoyama Gakuin University, 6-16-1 Chitosedai, Setagaya, Tokyo 157, Japan (takemoto@me.aoyama.ac.jp). Yasuhisa Hayashi is with Faculty of Engineering, Shizuoka University, Shiroyama, Hamamatsu, Shizuoka, Japan and Kanji Ono is with Department of Materials Science and Engineering, University of California, Los Angeles, Los Angeles, CA 90095-1595, USA (ono@seas.ucla.edu).

fields, but has not been used in the field of acoustic emission (AE). The WT is useful in analyzing the frequency components of an AE signal as a function of time and in separating valid signals from noise. Wavelet coefficients (or spectral intensities at a given time) in the time-frequency coordinate can be presented as a contour map (namely, a spectrogram or a voiceprint) or as a three-dimensional projection. These plots illustrate characteristic features of the signals at a glance.

Acoustic emission monitoring is useful to study the fracture modes and kinetics in various materials, especially in fiber reinforced composites. In glass fiber reinforced composites (GFRPs), many types of fractures can be distinguished by careful AE source waveform simulation studies (Suzuki et al., 1993, 1996). Some of the present authors developed a ten-channel AE monitoring system with two digitizers for conducting a wavelet transform study. We used this system to classify observed AE signals and to examine the correspondence of the classified signals with the fracture mode identified by the source simulation approach.

As a demonstration of WT, we performed the WT of AE signals obtained by using resonant-type AE sensors. Even though the waveforms of such signals are strongly affected by the sensor characteristics, we can successfully distinguish the signals due to fiber fracture, matrix crack and Mode-I or Mode-II disbonding in GFRPs by the wavelet transform. Of course, the assignment of specific fracture mechanisms still requires the source simulation analysis, but it is shown that WT is a powerful new analysis method in evaluating AE signals.

2. Wavelet Transform

Wavelets and wavelet transforms are a relatively new topic in signal processing. The theory continues to evolve and their applications are expanding to various fields as noted previously. We are interested in the application of the wavelet transform (WT) to the time-frequency analysis of AE signals and a brief introduction of WT is given below.

The Fourier transform (FT) is used widely in signal analysis. The Fourier transform and its inverse are defined as follows:

$$S(\omega) = \int s(t) \exp(-i\omega t) dt \quad (1)$$

$$s(t) = (1/2\pi) \int S(\omega) \exp(i\omega t) d\omega \quad (2)$$

where $S(\omega)$ is the Fourier transform of a signal $s(t)$. The FT of $s(t)$, $S(\omega)$, is a function independent of time and describes the signal in the frequency domain (in terms of $\omega = 2\pi f$). Here, $\exp(i\omega t) = \cos \omega t + i \sin \omega t$ is the basis functions. This means that any given signal can be constructed

by a combination of the 'basis functions' (in analogy to the description of an arbitrary vector via a weighted combination of the "basis vectors"). $S(\omega)$ is the weight at frequency ω . We can also describe the FT as the weight in the decomposition of the signal $s(t)$ into the basis functions $\exp(-i\omega t)$.

In the case of the FT, these basic functions are complex sinusoids, $\exp(i\omega t)$, that exist for $-\infty \leq t \leq \infty$. Thus, the Fourier transform is ideal for the analysis of stationary signals (signals whose statistical properties do not change with time). When $s(t)$ is short as in most AE signals, we assume a periodicity in the application of the FT.

For the analysis of non-stationary or transient signals, we need another method that transforms a signal into a joint time-frequency domain. The windowed or short-time Fourier transform (WFT or STFT) makes this possible. Gabor (1946) originated WFT as an extension to the classical Fourier transform. Here, $s(t)$ is windowed by a window function $w(t)$ around time τ or $w(t - \tau)$, then the FT is performed. As the window function is shifted in time by changing τ over the whole signal and consecutive overlapped transforms are performed, we can describe the frequency spectrum of the signal as a function of time. This is commonly called the signal spectrogram. The WFT of $s(t)$ is defined as

$$[WFTs](\omega, \tau) = \int s(t) w(t - \tau) \exp(i\omega t) dt \quad (3)$$

When the window function is Gaussian,

$$w(t - \tau) = \exp[-(t - \tau)^2/\sigma^2] \quad (4)$$

with a constant σ , the WFT is also called Gabor transform. (If we use the same type of notation as in equation (3) above, the left-side of equation (1) can be written as $[FTs](\omega) = S(\omega)$.)

It is possible to describe the WFT as the decomposition of the signal $s(t)$ into the windowed basis functions $w(t - \tau) \exp(i\omega t)$; i.e., these basis functions are complex sinusoids, $\exp(i\omega t)$, windowed by the function $w(t)$ centered around time τ . Three examples from a set of the windowed basis functions are given in Fig. 1c, which are formed by the product of cosine waves in Fig. 1a and the window functions in Fig. 1b. The length of these basis functions is constant as the shape of the Gaussian window function remains the same. The FT of the windowed basis functions are shown in Fig. 1d. These clearly indicate that the frequency resolution remains constant; this also implies that the relative resolution improves at higher frequency.

The windowing has a detrimental effect upon the frequency resolution in comparison to the infinitely extended sine or cosine basis functions. On the other hand, a short window results in a good resolution in time. This is a con-

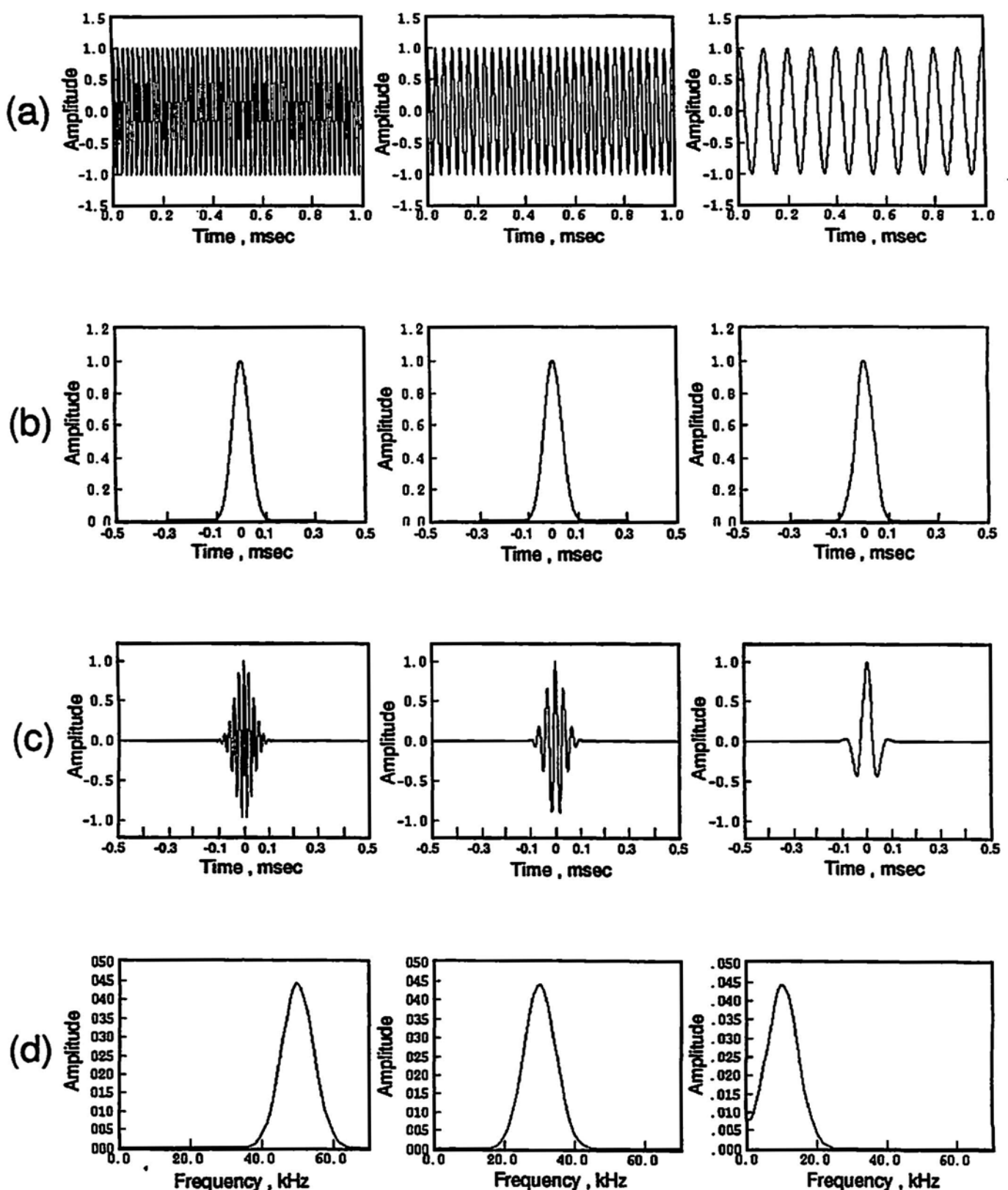


Fig. 1 The windowed or short-time Fourier transform. (a) Continuous waves, (b) Windows, (c) The product of (a) and (b), (d) Fourier transform of (c).

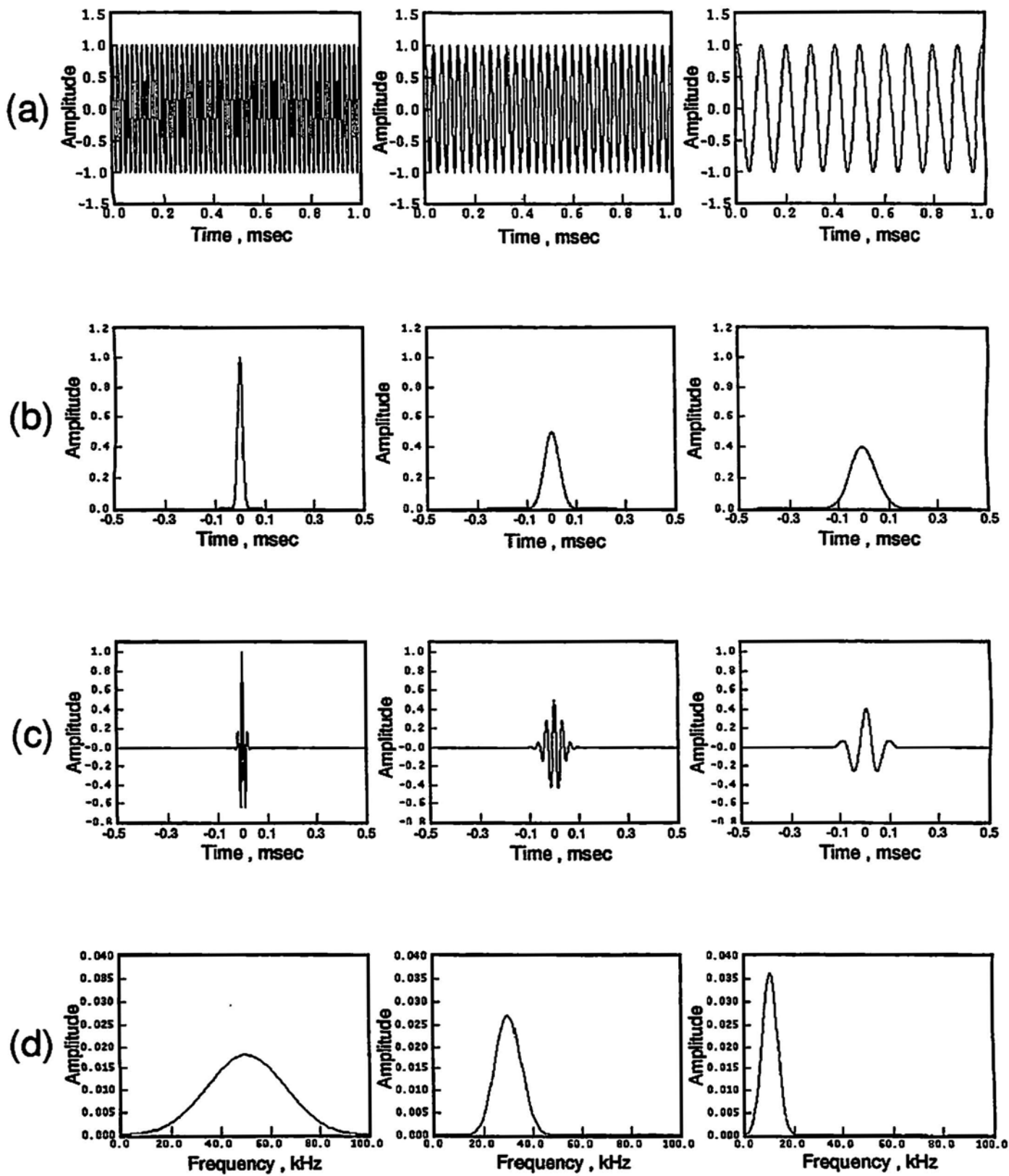


Fig. 2 The wavelet transform. (a) Continuous waves, (b) Windows, (c) The product of (a) and (b), (d) Fourier transform of (c).

sequence of the uncertainty principle. If Δt is the transform resolution in the time domain and $\Delta\omega$ is the transform resolution in the frequency domain, the uncertainty principle can be written in the WT literature as

$$\Delta t \Delta\omega = 1/2. \quad (5)$$

Both of these factors remain constant in a WFT analysis, resulting in the WFT covering the time-frequency plane with a uniform array of resolution squares. Despite such limitations, the WFT is useful in many problems where time-frequency characteristics are required.

The wavelet transform (WT) is a further extension of WFT. Instead of the constant window shape of the basis functions of the WFT, the basis functions of the WT are scaled with respect to frequency. Figure 2c shows the fundamental basis function and two scaled basis functions. In analogy to Fig. 1, these are formed by multiplying cosine (Fig. 2a) and window (Fig. 2b) functions. Figure 2d shows the FT of the scaled wavelets. These indicate that the spectral width broadens at a higher frequency while a better frequency resolution is obtained at a lower frequency. In turn, the relative frequency resolution in WT remains constant. In WT, the amplitude is also scaled (the shorter in time, the higher in amplitude) as shown in Fig. 2c. These basis functions are short waves with limited duration; thus, the name "wavelet" is used. There are many different wavelets that can be used as the basis functions, although it is adequate for AE signal analysis to use Gabor wavelet or a Gaussian window function applied on $\exp(i\omega t)$. The real and imaginary parts of a Gabor wavelet are shown in Fig. 3a, whose FT is shown in Fig. 3b with the center frequency of 450 kHz in this example. The fundamental basis function is usually referred to as "mother wavelet", while the scaled versions are daughter wavelets.

Due to the scaling shown in Fig. 2, wavelets at high frequencies are of short duration (good time resolution) and wavelets at low frequencies are relatively longer in duration

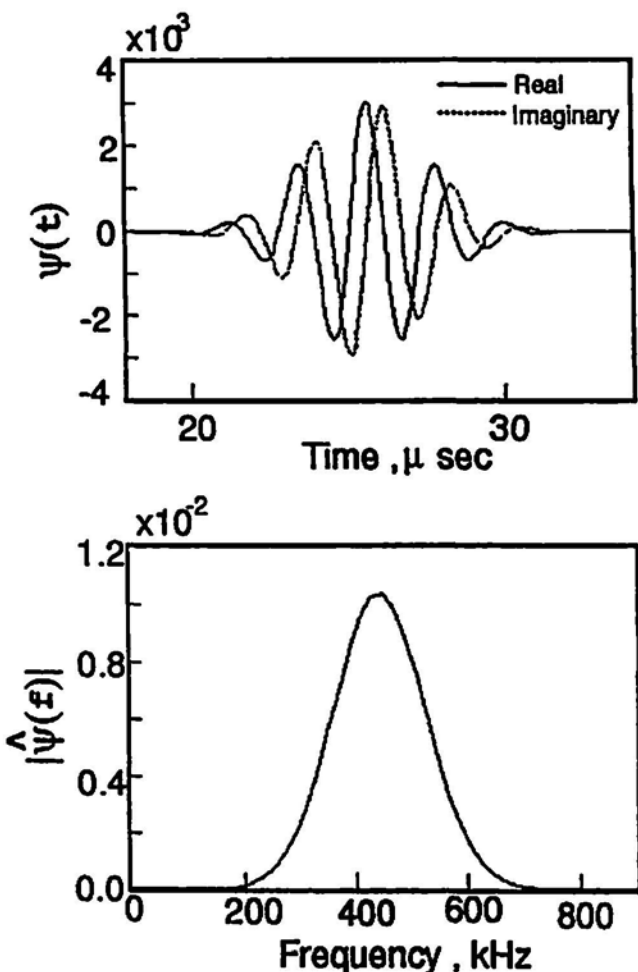


Fig. 3 (a) The real and imaginary parts of a Gabor wavelet. The center frequency is 450 kHz. (b) The Fourier transform of (a).

(good frequency resolution). This varying "window" structure of the WT is reflected in the resolution on the time-frequency plane by rectangles, as shown in Fig. 4a. The corresponding partition of the time-frequency plane in the case of WFT is represented by identical squares (Fig. 4b).

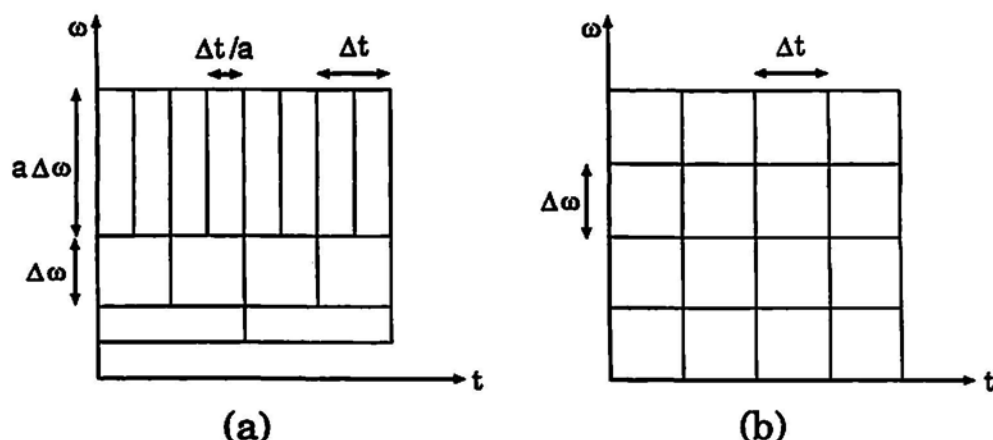


Fig. 4 (a) The rectangular resolution of the WT on the time-frequency plane. $\Delta\omega$ and Δt are the spectral and time width and a is the scaling parameter. (b) The corresponding square resolution of the WFT.

These variable window-length characteristics of WT are obviously suited to the analysis of signals containing short high-frequency components and extended low-frequency components, which are often the case for AE signals.

As the WFT decomposes a signal into the windowed basis functions, $w(t - \tau) \exp(i\omega t)$, the WT utilizes its basis functions, known as wavelets, and performs a decomposition of the signal $s(t)$ into a weighted set of scaled wavelet functions $\psi(t)$. In general, a wavelet $\psi(t)$ is a complex valued function. A general wavelet function is defined as

$$\psi_{a,b}(t) = |a|^{-1/2} \psi[(t - b)/a] \quad (6)$$

The function $\psi(t)$ is the mother wavelet with the scale parameter a and the shift parameter b and provides a set of localized functions both in frequency and time. The scale parameter, a , gives the width of window and consequently frequency as the mother wavelet is expanded or compressed in time. This can be understood from the following Fourier transform of the mother wavelet (equation (6) above);

$$[\text{FT}\psi_{a,b}](\omega) = \hat{\psi}_{a,b}(\omega) = |a|^{1/2} \hat{\psi}(a\omega) e^{-i\omega b} \quad (7)$$

This effect of the scale parameter in the frequency domain is illustrated in Fig. 5.

The shift parameter, b , determines the position of the window in time and thus defines which part of the signal $s(t)$ is being analyzed. It is common in the WT analysis that the frequency variable ω is replaced by the scale variable a and the time-shift variable τ is represented by b .

The wavelet transform of $s(t)$ is then defined by:

$$[\text{WT}s](a, b) = \int_{-\infty}^{\infty} \psi_{a,b}^*(t) s(t) dt \quad (8)$$

where ψ^* is the complex conjugate of the wavelet function defined by equation (6).

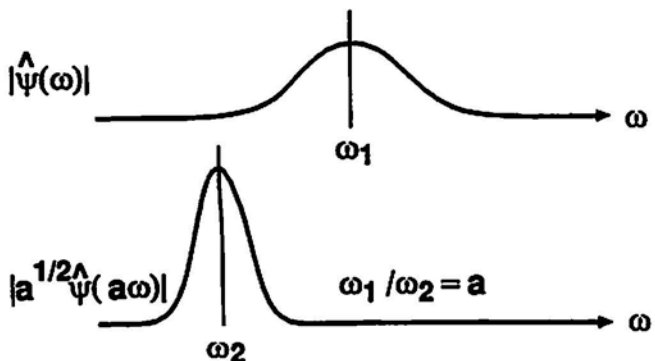


Fig. 5 The effect of the scale parameter in the frequency domain.

In this work, we use the Gabor wavelet based on the Gaussian function, given as equation (4). The mother wavelet and its Fourier transform are given as:

$$\begin{aligned} \psi(t) &= \pi^{-1/4} \left(\frac{\omega_p}{\gamma} \right)^{1/2} \exp \left[-\frac{t^2}{2} \left(\frac{\omega_p}{\gamma} \right)^2 + i\omega_p t \right] \\ \hat{\psi}(\omega) &= (2\pi)^{1/2} \pi^{-1/4} \left(\frac{\omega_p}{\gamma} \right)^{1/2} \exp \left[-\frac{t^2}{2} \left(\frac{\omega_p}{\gamma} \right)^2 (\omega - \omega_p)^2 \right] \end{aligned} \quad (9)$$

Here, ω_p is the center frequency and γ is a constant taken as $\gamma = \pi (2/\ln 2)^{1/2} = 5.336$. From the Fourier transform, we find the half-value frequency width of the Gabor wavelet to be $2\omega_p/\gamma$ and the half-value time width to be $2\gamma/\omega_p$. The specific value of γ was chosen to nearly satisfy the so-called admissibility condition; i.e., the wavelet functions must satisfy the orthonormality condition.

Consider a typical digitized AE signal of the sampling interval of Δt_s and the sampling length of N ; the corresponding angular Nyquist frequency is $\pi/\Delta t_s$. In order to obtain the wavelet transform of such a signal, we select the center frequency, ω_p , of the mother wavelet as $(2)^{1/2} \pi/\Delta t_s$. For the frequency range of 10 kHz to 2 MHz to be covered with adequate resolution, we need to use 20 to 40 scale parameters or a_n with $n = 0$ to 19 to 39. The scale parameters are selected as $a_n = \alpha^n$, with $\alpha = 2^{1/4}$. Other suitable values of α include $2^{1/5}$ and $2^{1/6}$, which cover wider ranges of frequency with the same value of n . The shift parameters, b_m , are chosen as a multiple of the sampling interval of Δt_s ; i.e., $b_m = m\Delta t_s$. Here, $0 \leq m \leq N/2$, in order to avoid the WT calculation extending beyond the sampling length. Frequency-defining parameter, n , in the above wavelet transform can be converted to frequency by $f^1 = 2^{(n+2)/4} \Delta t_s$, since the n -th daughter wavelet has the center frequency of ω_p/a_n .

Results of WT of a signal are a collection of wavelet coefficients; each wavelet coefficient for a given set of the scale (or frequency) and shift (or time) parameters, a and b , which can also be represented by n and m . The results are often represented as a contour map on a $\log(a)-b$ plane with the gray levels (or false color levels) representing the wavelet coefficients or respective intensities of the transform at points in the $\log(a)-b$ plane. The contour profile is basically the same as the voiceprint, and shows how the signal intensity of a particular frequency changes with time. Using a logarithmic scale-parameter axis allows a large range of frequency to be simultaneously displayed. Most discussion will be done using the contour map in the following. The original contour map is in color, showing peak height in false color, but will be presented in gray-scale diagram. Here, white represents the zeroth level wavelet coefficient, and black part the highest with different shades of gray in between. Alternate display method is the use of three-dimensional plot or bird's-eye view with a staggered graphs

of the intensity-time plots. This type of presentation is helpful in gaining general trends of time-frequency characteristics. The bird's-eye view of WT coefficients shows some characteristic features well, depending on the waveform type and perspective, but is difficult to present in a limited space. A suitable viewing angle may be required as certain details become hidden.

Examples of AE waveforms and their FT and WT are shown in Fig. 6. The wavelet profile is represented in the third row as a bird's-eye view and in the fourth row as a contour map. It shows in detail how different frequency

components change with time in contrast to the FT shown in the second row.

Computer program for the wavelet transform is given in Appendix. This is written for the Gabor wavelet.

3. AE Signals from GFRP under Tensile Loading

In order to examine the utility of wavelet transform for AE signal classification, it was applied to AE signals from a GFRP specimen. We prepared a unidirectional GFRP

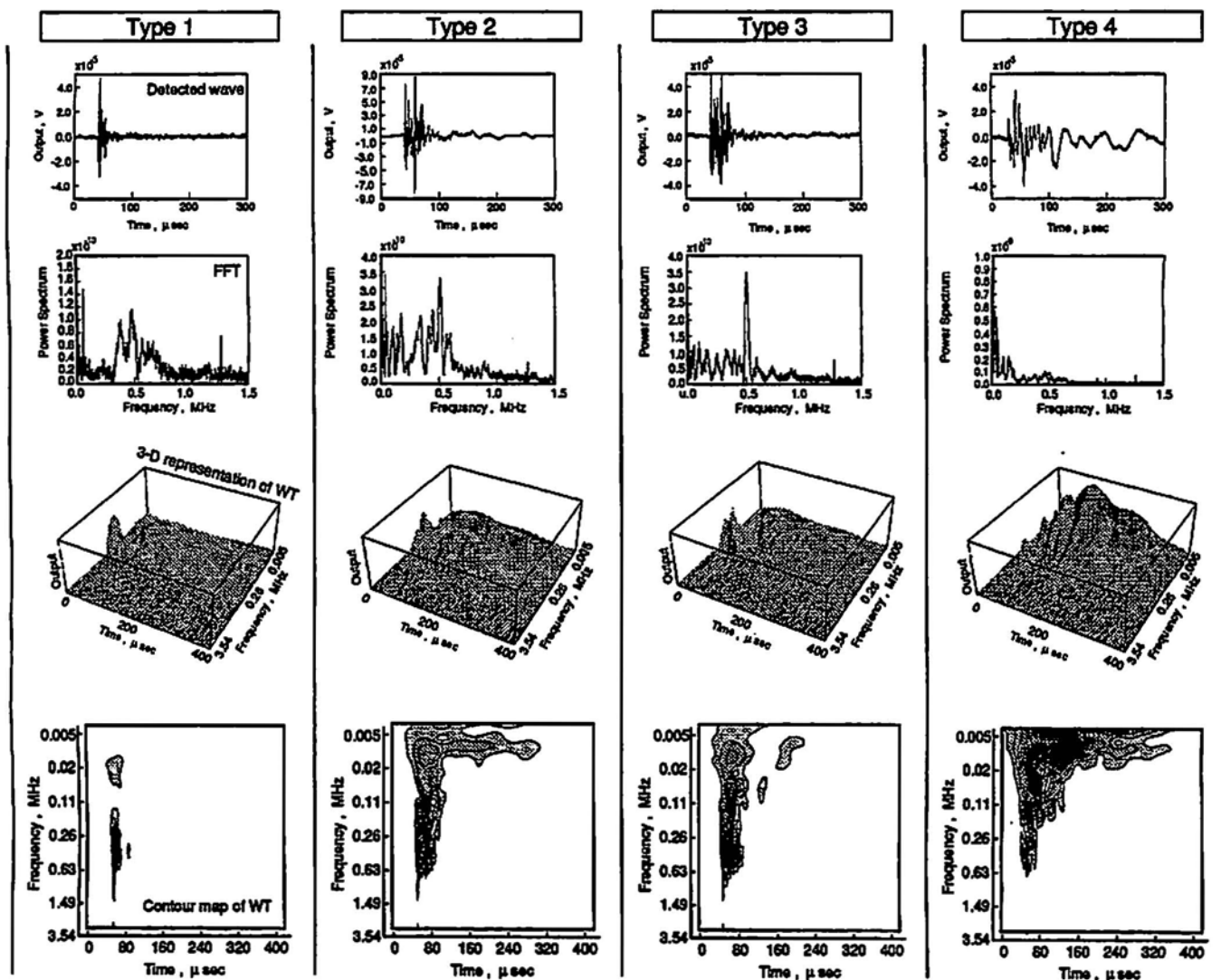


Fig. 6 Examples of AE waveforms and their FT and WT.

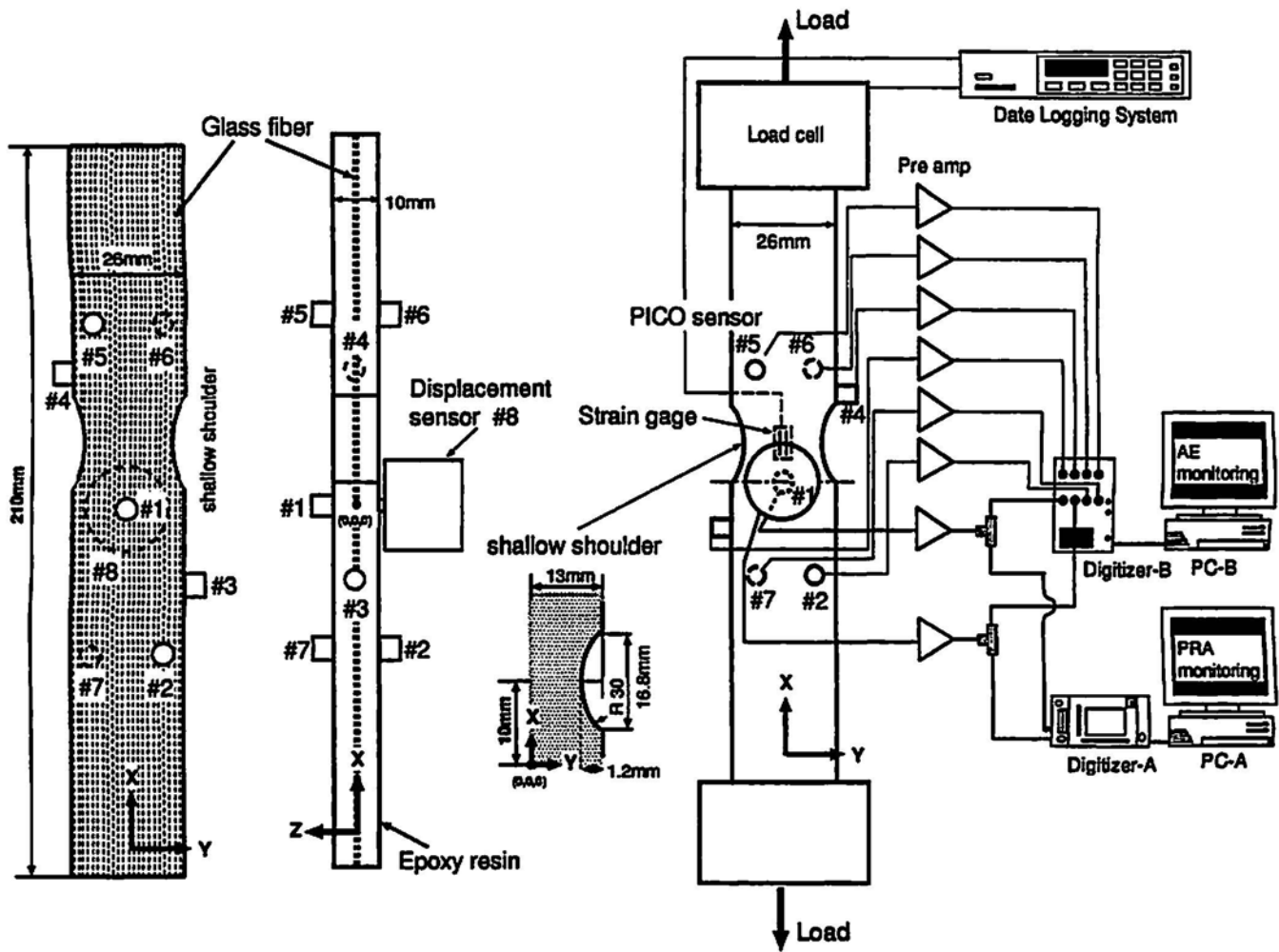


Fig. 7 Details of a unidirectional GFRP specimen with the fiber position and sensor placements. Schematic diagram of eight sensors and a ten-channel AE monitoring system is also given.

specimen with the fiber orientation shown in Fig. 7. Six thousand E-glass fibers were molded in epoxy (6 parts Epicote 828 and 4 parts Epicote 878, supplied by Shell Epoxy Co. Ltd). Glass fibers, 13 μm in diameter, were treated with silane coupling agent prior to the molding and spread uniformly on the X-Y plane at the mid-thickness. A reduced section with shallow shoulders was included at the middle part of the specimen to concentrate the fracture events. The origin of the coordinate is at the central point of the specimen. Eight sensors and a ten-channel AE monitoring system were used. Seven sensors (#1 to #7) with 3-mm aperture diameter (Dungun PICO) have mainly been used for the source location and fracture mode analysis based on the radiation pattern of the P-wave. The #8 sensor was a displacement sensor with a conical PZT element (1 mm tip-diameter). It was mounted on the opposite side of the #1 sensor. This sensor was utilized to obtain the source waveform (Suzuki et al., 1994, 1996). For the present WT study, the output of #1 sensor was utilized.

Using the calibration method of surface-impulse deconvolution (ref), we found that PICO sensors measured the velocity component of the out-of-plane displacement, while the displacement sensor detected the out-of-plane displacement with the sensitivity of $6.01 \times 10^7 \text{ V/m}$. Two separate digitizers (Digitizer A and B) were used because the sampling conditions for the wavelet transform and source simulation and for the source location/radiation pattern analyses were different. The outputs of #1 and #8 sensors were recorded on both digitizers. The outputs of #1 and #8 sensors were amplified by a 40-dB preamplifier (NF Circuit Block Co. Ltd., Type 9913) and then digitized at 200-ns sampling interval and 8 bit with 4096 sampling points by the digitizer A (Tektronix, RTD 720, H310). This set of data was used for the wavelet transform and source simulation. The outputs of #1 to #8 sensors were amplified by the same amplifier and digitized at 50 ns interval and 10 bit with 1024 sampling points by the digitizer B (Autonics, APC-510). The data on 8 channels of digitizer B was used for the source location and P-wave radiation pattern analyses. This

monitoring system enables us to compare the wavelet transform results with the fracture mode deduced by the source simulation and radiation pattern analyses. Detail for the latter signal processing methods can be found elsewhere (Suzuki et al., 1996).

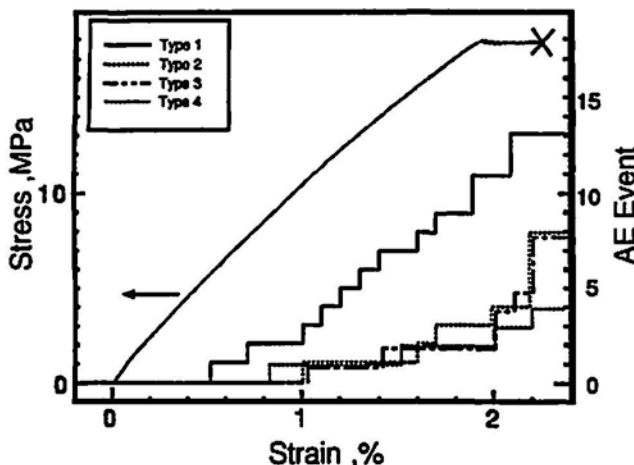


Fig. 8 The stress-strain curve and the cumulative AE events vs. strain for four types of AE signals.

4. Results and Discussion

Figure 8 shows the stress-strain curve, and the cumulative AE events vs. strain. The specimen was stressed at a constant strain rate of 0.05%/min to 18 MPa (or a strain of 1.9%), and then held at this stress. After holding this stress for 42 min, the specimen fractured with the final fracture strain of 2.3%. We observed 46 AE events in all. Source location was possible for 33 events.

By examining the waveforms, their power spectra and wavelet transform of the 33 events, we classified the observed AE signals into four types; i.e., Types 1 to 4. Type 1 AE events were observed from small strains and their number increased almost linearly with stress, but little further increase was observed during the stress hold. AE events of Types 2 and 3 increased from 1% strain, but at lower emission rates than that of Type 1. Both Types 2 and 3 continued to increase after the stress hold started. Type 4 AE events increased from 0.8% strain, but its emission rate was the lowest.

Figure 9 illustrates four typical Type-1 signal waveforms from sensor #1 (the upper row), the power spectrum of the entire waveform via FFT (the second row), as well as FFT of the first 20 μ s following the sharp rise of the signal (the third row). The fourth and bottom rows show the wavelet coefficients as the 3-D representation and contour map, respectively. Type 1 waveforms are short and of a typical "burst type". The FFT indicates their main power in the frequency range from 0.3 to 0.6 MHz with dips at about 0.5 MHz. The power spectra for the main part of the signals

have similar features. The WT contour maps best show the characteristic features of the waveforms. Type 1 waveforms show that high frequency components of the signals last for a short time with the appearance of a vertical line at left side in the frequency range from 0.1 to 1.5 MHz. Some low frequency components are present and extend for longer periods. The bird's-eye view of wavelet coefficients shows a single sharp peak.

Four typical Type-2 signals are given in Fig. 10. As in the previous figure, waveforms from sensor #1 (the upper row), the power spectrum of the entire waveform via FFT (the second row), FFT of the first 20 μ s following the sharp rise of the signal (the third row), the wavelet coefficients in the 3-D representation (the fourth row) and as the contour map (the bottom row), respectively. Characteristic features are as follows: The frequency spectra again show high intensity from 0.3 to 0.6 MHz, but with a peak at 0.5 MHz and a higher intensity below 0.1 MHz. The WT contour maps reveal that higher frequency components occur at two distinct time periods (indicated by two vertical lines) and that a weak low frequency component lasts continuously for 250 to 300 μ s. The bird's-eye view of wavelet coefficients shows split sharp peaks plus an extended range of hills.

Four typical Type-3 signals are given in Fig. 11. The frequency spectra show a high intensity peak at 0.5 MHz. The short FFT spectra give a broader range of high intensity. The WT contour maps reveal that higher frequency components last longer than in Type-1. The two-vertical line feature seen in Type-2 is absent. The low frequency components appear at the same time as the high frequency components; i.e., at 30 to 120 μ s. A few islands of low frequency components also appear at later times. The bird's-eye view of wavelet coefficients shows a group of sharp peaks plus a broad-top mountain. It is noted that the contour map shows a clear profile difference in the lower frequency range for Types 2 and 3, while both the waveforms and frequency spectra of these signals closely resemble each other.

Frequency spectrum of Type 4 is different from any other type as can be seen in Fig. 12. It contains higher intensity in the frequency region lower than 0.5 MHz with the highest intensity occurring below 0.02 MHz. Both WT contour maps and bird's-eye views reveal a broad peak at the low frequency region.

These examples show that the characteristic features of waveforms are best revealed by the WT contour maps and by the bird's-eye view of wavelet coefficients. Differences in these waveforms exist and can be recognized, but distinction is at times hard to discern. The WT analysis can separate different waveform types at a glance. The main drawback of the WT analysis is the length of computation time in comparison to nearly instantaneous calculation of FFT.

Type 1

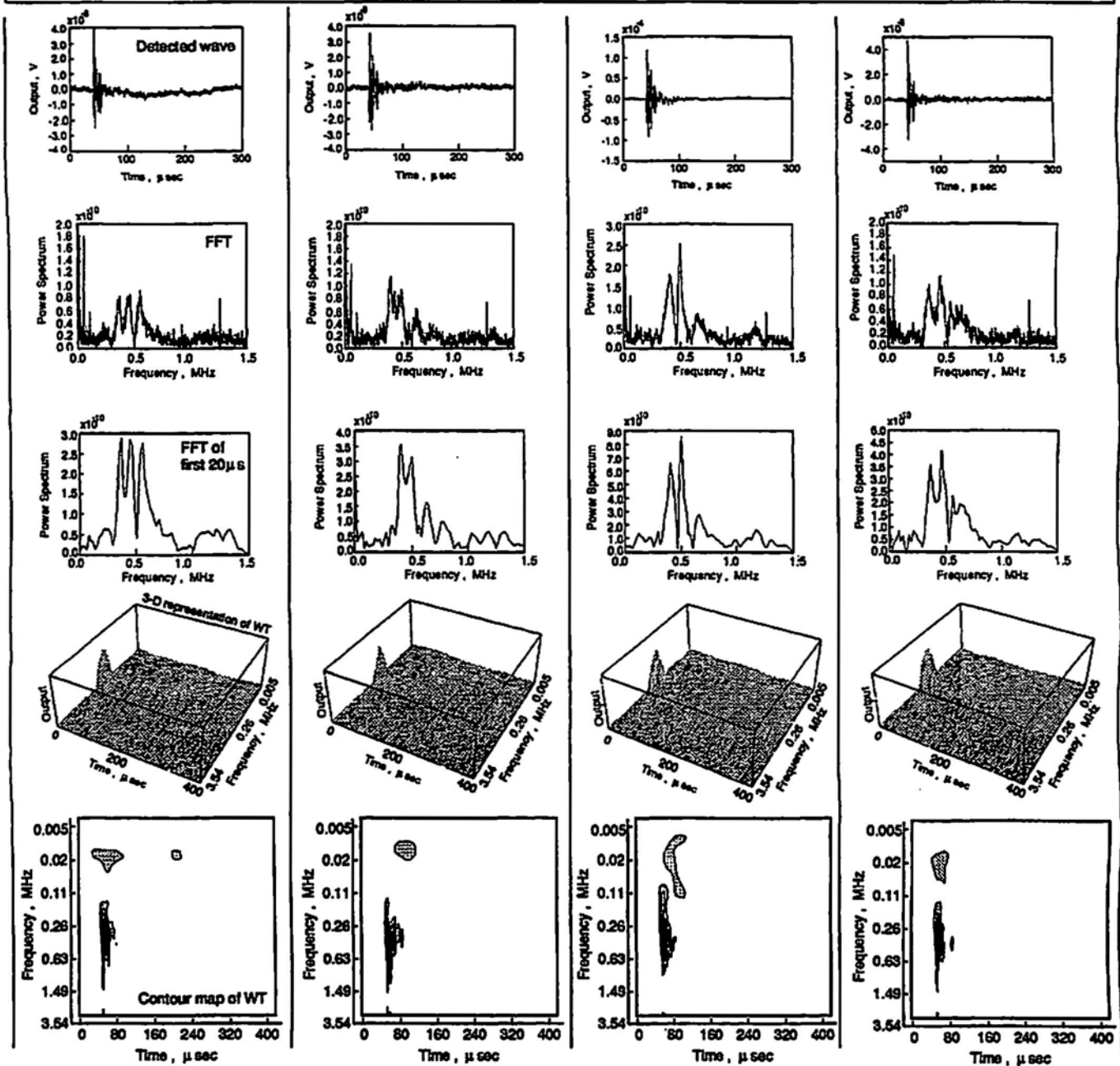


Fig. 9 Four typical Type-1 signal waveforms from sensor #1 (the upper row), the power spectrum of the entire waveform via FFT (the second row), FFT of the first 20 μ s following the sharp rise of the signal (the third row). The fourth and fifth rows show the wavelet coefficients as the 3-D representation and contour map, respectively.

In order to identify the fracture mode of the four types of AE signals observed, we conducted the source location, radiation pattern and source simulation analyses. Figure 13 represents the source locations of 33 events in X-Y and Y-Z diagrams. Four symbols, filled diamonds, open circles, open squares and Xs, represent Type 1, 2, 3 and 4 signals, respectively. The source locations of Type 1 signals (marked by a,b, and c) are scattered over the X-Y plane, but they all lie almost on the fiber-bundle plane. Most of Type 2 signals, (d,e, and f), and Type 3 signals, (g,h, and i), are located in the matrix and near the outer edge of the reduced

section. These indicate that Type 1 signals are emitted by the fiber fracture, while Type 2 or 3 signals are by the matrix crack. The source location of Type 4 signals, (j and k), are located at the surface where a strain gauge was bonded, and appeared to be emitted by the exfoliation of the strain gauge. In this sense, Type 4 signals are noise.

These signals were also subjected to the radiation pattern and source simulation analyses in order to identify the fracture mode (Suzuki et al., 1994, 1996). From these analyses along with the above source locations, we attribute

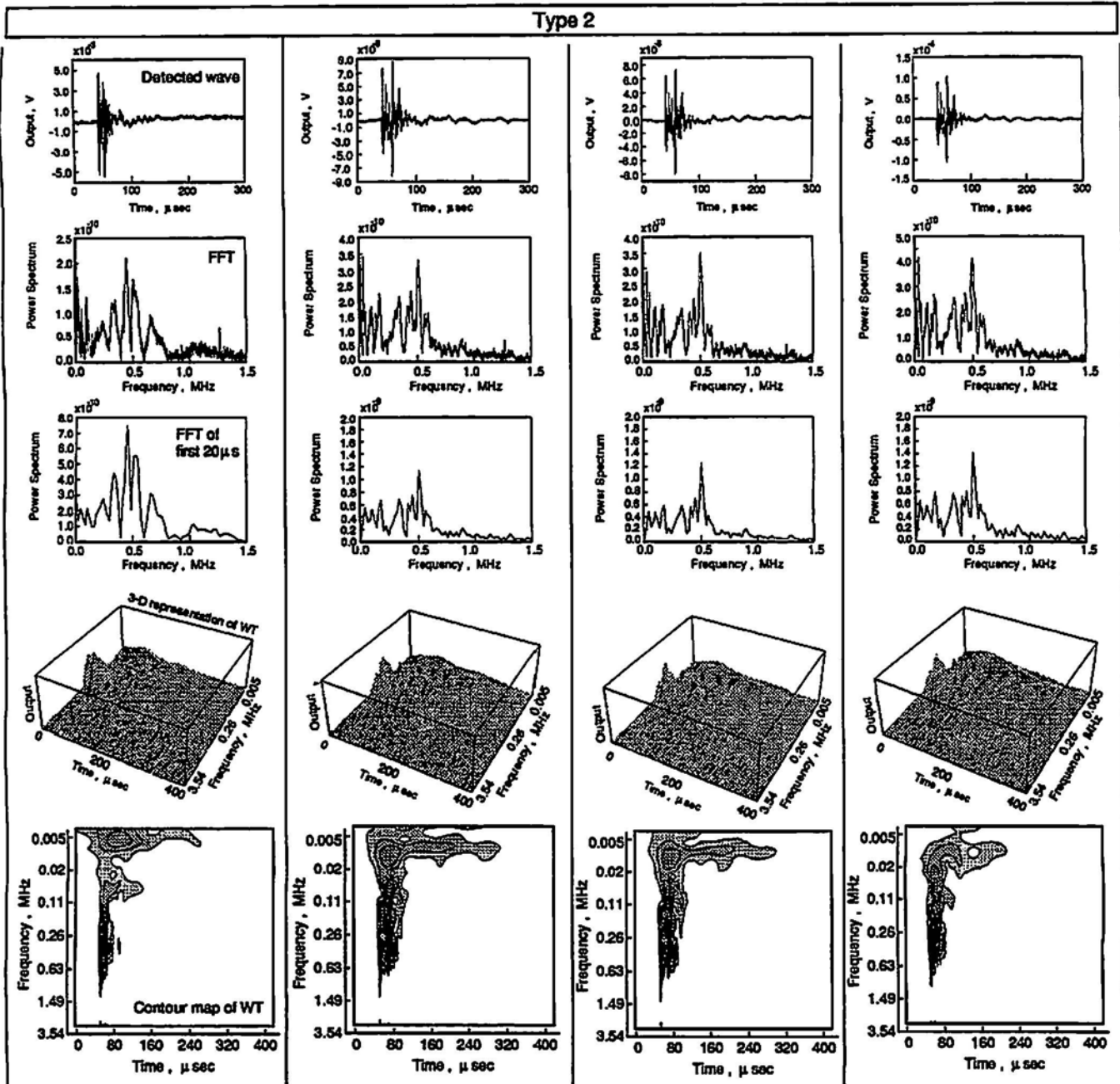


Fig. 10 Four typical Type-2 signal waveforms from sensor #1 (the upper row), the power spectrum of the entire waveform via FFT (the second row), FFT of the first 20 μ s following the sharp rise of the signal (the third row). The fourth and fifth rows show the wavelet coefficients as the 3-D representation and contour map, respectively.

Type 1 signals to Mode-I fiber fractures, Type 2 and 3 to multiple Mode-I matrix cracks, and Type 4 to the Mode-II exfoliation of the strain-gauge base.

5. Conclusions

Wavelet transform of AE signals provides plots of their frequency spectra as a function of time. It is useful in the recognition of AE signal features through 2-dimensional contour maps and 3-dimensional projections of wavelet coefficients. Computer programs for wavelet transform have

been written and incorporated into a ten-channel AE monitoring and signal processing system. As a test of the utility of the system, it was used to examine the AE signals from a model GFRP sample. The wavelet transform and source analysis procedures for the same set of AE signals were applied and the results obtained are presented.

- We developed a set of computer programs for the wavelet transform with Gabor wavelet, as given in Appendix. These can be used for the analysis of AE signals as well as other transients.

Type 3

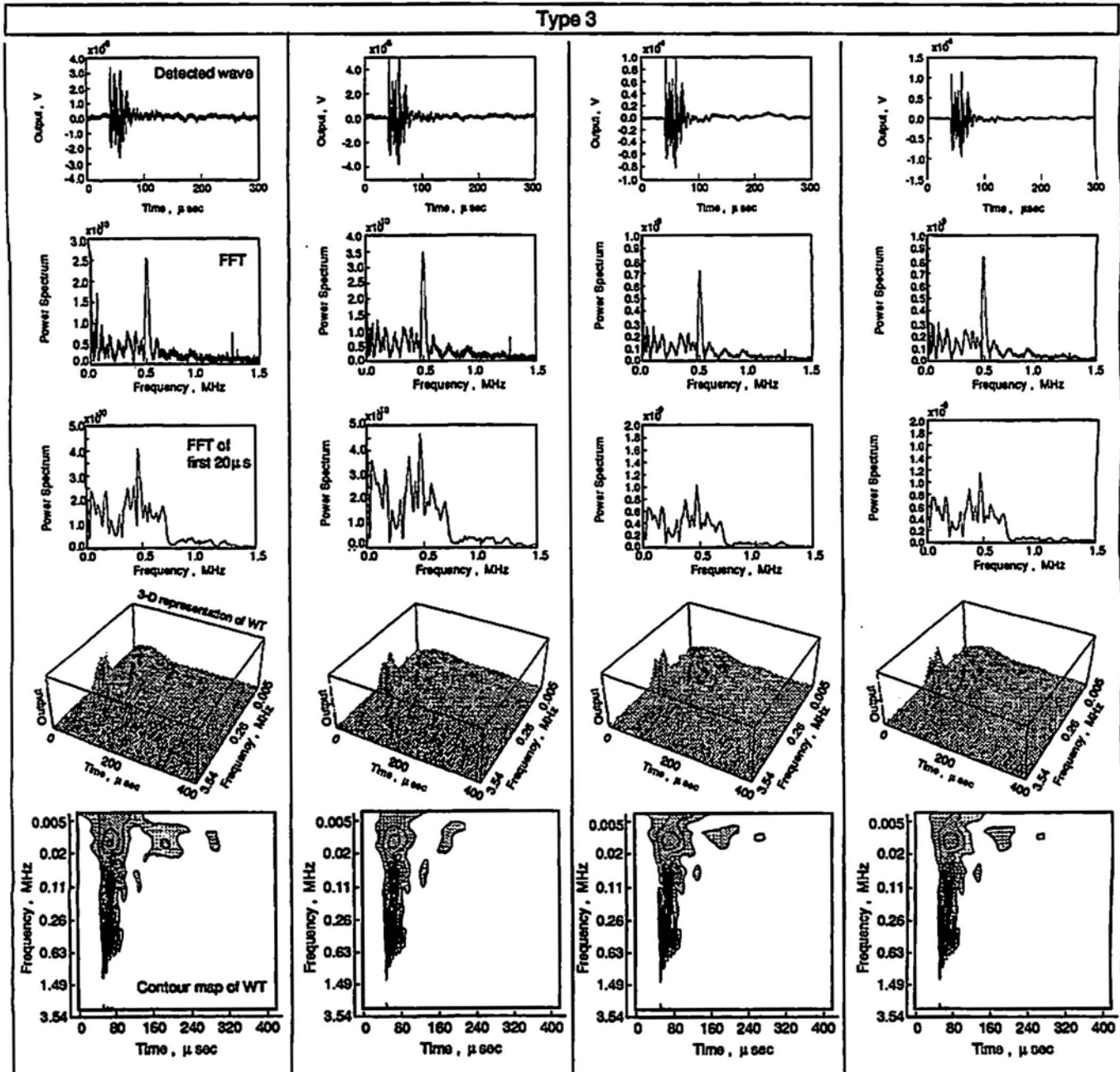


Fig. 11 Four typical Type-3 signal waveforms from sensor #1 (the upper row), the power spectrum of the entire waveform via FFT (the second row), FFT of the first 20 μ s following the sharp rise of the signal (the third row). The fourth and fifth rows show the wavelet coefficients as the 3-D representation and contour map, respectively.

- The characteristic features of waveforms are best revealed by the WT contour maps and by the bird's-eye view of wavelet coefficients. The WT results can separate different waveform types at a glance. The main drawback of the WT analysis is the length of computation time.
- The wavelet transform was applied to AE signals emitted during tensile loading of a model unidirectional GFRP and allowed us to classify the signals into four patterns. By applying the source location, radiation pattern and source simulation analyses, the four signal types classified by the

wavelet transform were correlated to the Mode-I fiber fracture, the Mode-I matrix crack and the Mode-II disbonding.

Acknowledgment

We acknowledge the assistance of undergraduate students, Messrs. N. Kugizaki, K. Ousika and M. Nemoto. The authors are also grateful to Showa Kobunsi Co. for providing us with epoxy resin and to Teitsu Densi Co. for a special PZT sensor.

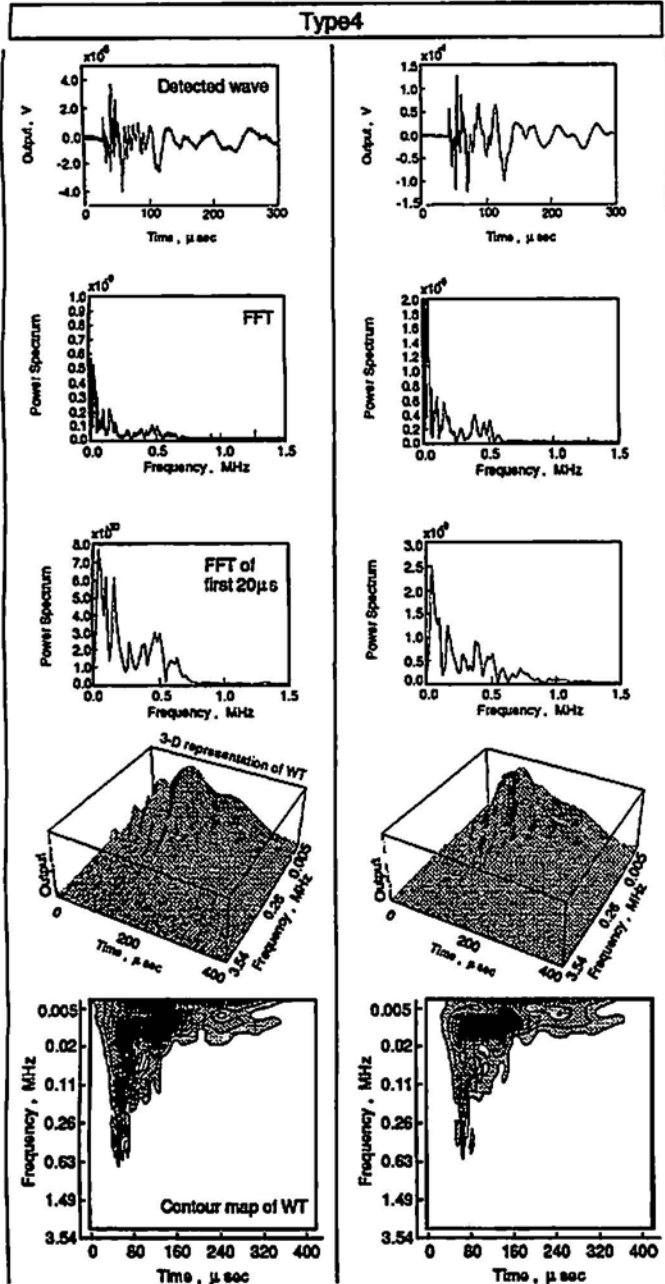


Fig. 12 Two typical Type-4 signal waveforms from sensor #1 (the upper row), the power spectrum of the entire waveform via FFT (the second row), FFT of the first 20 μ s following the sharp rise of the signal (the third row). The fourth and fifth rows show the wavelet coefficients as the 3-D representation and contour map, respectively.

References

R.M. Belchamber, D. Betteridge, Y.T. Chow, T. Lilley, M.E.A. Cudby and D.G.M. Wood (1985), "Evaluation of Pattern Recognition Analysis of Acoustic Emission from Stressed Polymers and Composites", *J. Acoustic Emission*, 4(4), 71-83.

R.W.Y. Chan, D.R. Hay, V. Caron, M. Hone and R.D. Sharp (1985), "Classification of Acoustic Emission Signals Generated during Welding", *J. Acoustic Emission*, 4(4), 115-123.

C.K. Chui (1992), *Introduction to Wavelet*, Academic Press, New York.

I. Daubechies (1992), *Ten Lectures on Wavelet*, SIAM, Philadelphia.

G. Kaiser (1994), *A Friendly Guide to Wavelets*, Birkhäuser, Boston.

Y. Mayer (1992), *Wavelet and Operators*, Cambridge University Press, Cambridge.

R.B. Melton (1982), "Classification of NDE Waveforms with Autoregressive Models", *J. Acoustic Emission*, 1(4), 266-270.

M. Ohtsu and K. Ono (1984), "Pattern Recognition Analysis of Magnetomechanical Acoustic Emission Signals", *J. Acoustic Emission*, 3(2), 69-80.

M. Ohtsu and K. Ono (1987), "Pattern Recognition Analysis of Acoustic Emission from Unidirectional Carbon Fiber-Epoxy Composite by Using Autoregressive Modeling", *J. Acoustic Emission*, 6(1), 61-71.

H. Suzuki, K. Takemoto and K. Ono (1993), "A Study of Fracture Dynamics in a Model Composite by Acoustic Emission Signal Processing", *J. Acoustic Emission*, 11(3), 117-128.

H. Suzuki, K. Takemoto and K. Ono (1996), "The Fracture Dynamics in a Dissipative Glass Fiber/Epoxy Model Composite with AE Source Wave Analysis", *J. Acoustic Emission*, 14(1), 35-50.

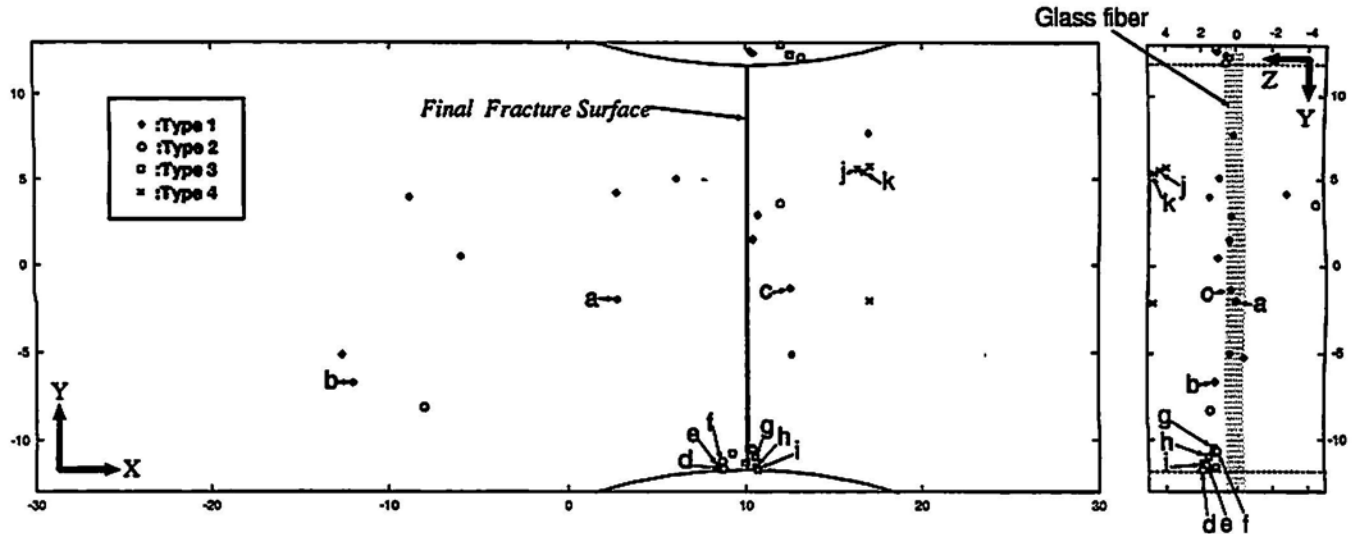


Fig. 13 The source locations of 33 AE events in X-Y and Y-Z diagrams. Four symbols, filled diamonds, open circles, open squares and Xs, represent Type 1, 2, 3 and 4 signals, respectively.

Appendix

Yasuhisa Hayashi

The author is affiliated with Faculty of Engineering, Shizuoka University, Shizuoka, Japan. (hayashi@sys.eng.shizuoka.ac.jp)

```
*****
The Program for Wavelet Transform

Usage: wavelet [-Nn][-Ssize] filename

      n:      n parameter number
      size:   output data size
              (This size can be reduced.)
      filename: output file name
*****
```

```
#include <stdio.h>
#include <math.h>
#include "complex.h"

#define MAXDATASIZE 4096 /* Max size of data */

complex gabor(), citg(), calcwavelet();
static char fname[50];

main(argc, argv)
int argc;
char **argv;
{
    char *p, *ifile, *pname = *argv;
    int N, osize;
```

```
N = 0;
osize = 0;

strcpy(fname, "out");
while(--argc && **++argv=='-'){
    p = *argv;
    switch(*++p){
        case 'n': case 'N':
            N = atoi(++p);
            break;
        case 'f': case 'F':
            strcpy(fname, ++p);
            break;
        case 'S': case 's':
            osize = atoi(++p);
            break;
        default:
            usage(pname);
    }
}
if(argc != 1)
    usage(pname);

ifile = *argv;
calcwavelet(ifile, N, osize);
}

usage(pname)
char *pname;
{
    fprintf(stderr, "Usage: %s [-Nn][-Ssize] filename\n",
            pname);
    exit(-1);
}
```

```

A = pow(2.0, N/4.0);

for(n=0; n<osiz; ++n){
    B = (double)n * dt;
    c = calc1wavelet(yfunc, siz, dt, A, B);
    cbuf[n].re = cabs(c);
    cbuf[n].im = 0.0;
    printf("%d: %e\n", n, cabs(c));
}
toadas(cbuf, osiz, dt);

complex calc1wavelet(yfunc, siz, dt, A, B)
complex *yfunpc;
int siz;
double dt, A, B;

int n;
complex wb;
static complex phi[MAXDATASIZE];

wavelet(phi,siz, dt, A, B);
for(n=0; n<siz; ++n)
    phi[n] = cprod(yfunc[n], conjg(phi[n]));
wb = citg(phi, siz, dt);
return(wb);

endif

wavelet(buf, siz, dt, a, b)
complex *buf;
int siz;
double dt, a, b;

int i, n;
double t, wp;
complex c;

c = cmplx(1.0/sqrt(a), 0.0);
wp = sqrt(2.0) * M_PI / dt;

for(n=0; n<siz; ++n){
    t = n * dt;
    buf[n] = cprod(c, gabor((t-b)/a, wp));
}

complex gabor(t, wp)
double t, wp;

double gam = 5.336;
double a;
complex b, c;

a = pow(M_PI, -1.0/4.0) * sqrt(wp/gam);
b = cmplx(-pow(t*wp/gam, 2.0)/2.0, wp*(t*wp/gam));

```

```

c = cprod(cmplx(a, 0.0), cexp(b));
return(c);
}

complex citg(buf, siz, dt)
complex *buf;
int siz;
double dt;
{
    int n;
    complex sum;

    sum = CNULL;
    for(n=0; n<siz; ++n)
        sum = csum(sum, buf[n]);
    sum.re *= dt;
    sum.im *= dt;
    return(sum);
}

toadas(cbuf,siz,dt)
complex *cbuf;
int siz;
double dt;
{
***** DATA OUTPUT ROUTINE

```

complex *cbuf: the pointer of output data
 arrangement
 int siz: output data size
 double dt: sampling interval

Prepare the data output routine for your convenience.
 The simplest routine is probably as follows;

```

int n;

for(n=0; n<siz; ++n)
    printf("%e: %e\n", cbuf[n].re, cbuf[n].im);

*****
}

getadas(fname, siz, cbuf, dt)
char *fname;
int siz;
complex *cbuf;
double *dt;
{
***** DATA INPUT ROUTINE

```

char *fname: the pointer of input data filename
 strings

int siz: input data size
 complex *cbuf: the pointer of input data buffer
 double *dt: the sampling interval of input data
 (You have to set these variables.)

Prepare the data input routine for your convenience.
 The simplest routine is probably as follows.

```

FILE *fp;
int n;
complex c;

fp = fopen(fname, "r");

for(n=0; n<siz; ++n){
    fscanf(fp, "%e%e", &c.re, &c.im);
    cbuf[n] = c;
}
*dt = 1e-6;
fclose(fp);

*****
}

fdsize(fname)
char *fname;
{
***** Return the input data size.

Ex.  return(1024);
*****
}
```